J. Fluid Mech. (1992), *vol.* 243, *pp.* 227–245
Printed in Great Britain

Further results for convection driven by the differential sedimentation of particles

By ROSS C. KERR[1] AND JOHN R. LISTER[2]

[1] Research School of Earth Sciences, Australian National University, GPO Box 4, Canberra, ACT 2601, Australia

[2] Institute of Theoretical Geophysics, Department of Applied Mathematics and Theoretical Physics, Silver Street, Cambridge CB3 9EW, UK

(Received 30 July 1991 and in revised form 23 March 1992)

When a well-mixed suspension of small particles is emplaced below a clear fluid whose density is greater than that of the interstitial fluid, but less than that of the bulk suspension, the subsequent settling of the dense particles releases buoyant interstitial fluid and drives convection in the overlying layer. Mixing of interstitial fluid and some entrained particles into the overlying fluid causes the density of the overlying fluid to evolve with time and changes the rate of descent of the interface between the sedimenting and convecting regions. These effects are investigated experimentally in a simple rectangular geometry using suspensions of spherical glass particles. It is found that the convecting region is well mixed in both composition and particle concentration and that the interfacial velocity may be predicted from the instantaneous (uniform) bulk density of the upper layer and the distribution of the particle settling velocities. In the case of an overlying density gradient, the convection does not extend through the depth of the overlying fluid but erodes the base of the gradient to form a well-mixed layer between the gradient and the sedimenting fluid. On completion of the first cycle of sedimentation-driven convection, sedimentation from this well-mixed layer produces further cycles of sedimentation-driven convection, which are of successively decreasing intensity and increasing duration. Whether the overlying fluid is uniform or stratified, both theory and experiment show that the particles that are lifted into the convection are smaller on average than those which settle at the base of the lower layer. Thus, when the lifted particles are eventually allowed to settle there is a discontinuity generated in the variation of the size distribution of particles with height in the final sedimented pile. This phenomenon may be an important mechanism for secondary layering in the deposits from turbidity currents and pyroclastic flows.

1. Introduction

In a recent paper, Huppert *et al.* (1991) (herein referred to as HKLT) examined the novel situation in which a suspension of particles is overlain by a fluid whose density ρ_U is greater than that of the interstitial fluid ρ_I, but less than that of the bulk suspension ρ_B (figure 1). The sedimentation of the particles in the suspension releases light interstitial fluid at the base of the overlying fluid, which can drive vigorous convection in this upper region. It was found experimentally that a sharp interface separates the upper convecting region from the suspension in the lower region, that this interface descends at a constant velocity and that there is undisturbed sedimentation in the lower region (figure 1*b*).

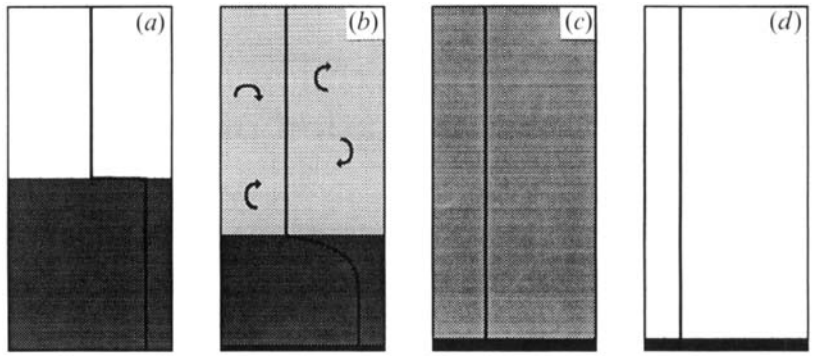

FIGURE 1. Schematic representation of the coupled sedimentation and convection, and the corresponding evolution in the bulk-density profile, that occur when a suspension is emplaced underneath a fluid whose density is greater than that of the interstitial fluid but less than that of the bulk suspension. (*a*) The initial configuration. (*b*) Settling of the particles releases light interstitial fluid, which drives vigorous convection in the overlying fluid. The convecting region is separated from a stagnant lower sedimenting region by a sharp interface. (*c*) Convection ceases once this interface has reached the floor. (*d*) The final configuration after the suspended sediment in the upper region is allowed to settle out.

HKLT used these qualitative observations to develop a quantitative theoretical description of the experimental results in which it was shown that the polydisperse nature of the suspension plays an important role in determining the rate of descent of the top of the sedimenting region. Owing to the differential sedimentation of particles away from the top of the initially well-mixed suspension, the bulk density in the suspension decreases from ρ_B far below the interface to ρ_I close to the interface (figure 2). Clearly, that part of the suspension with bulk density less than ρ_U is buoyant and must convect into the upper region. Further, some of the underlying suspension with density greater than ρ_U is entrained into the upper region by the convecting buoyant material, though such entrainment is limited by the constraint that the average density of the buoyant and entrained material together is less than ρ_U. The rate of convection and entrainment of part of the suspension into the upper region determines the rate of descent of the interface between the sedimenting and convecting regions. The interfacial velocity therefore depends principally on the distribution of particle settling velocities and on the vertical variation in the suspension of the buoyancy relative to the density of the upper layer. From these considerations of buoyancy and existing models of differential sedimentation, HKLT were able to explain the constant velocity of the interface and place upper and lower bounds on its value. (The reader is referred to the original paper for details of the calculation.) These bounds were found to bracket the majority of the experimental measurements; however, scatter in the experimental data and the occasional anomalous measurement clearly highlighted the need for further and more precise experiments, and this need provided part of the motivation for the present paper.

The tank used in the experiments of HKLT had a rather unusual geometry designed to minimize changes in the density of the overlying fluid during the experiment. The suspended particles were irregularly shaped carborundum grits which showed some tendency to coagulate, particularly in ionic solutions. In the experiments described herein, we employed a simple rectangular tank and spherical glass particles which showed no tendency to coagulate. In these simplified experiments, the variability in the experimental results was much reduced and we

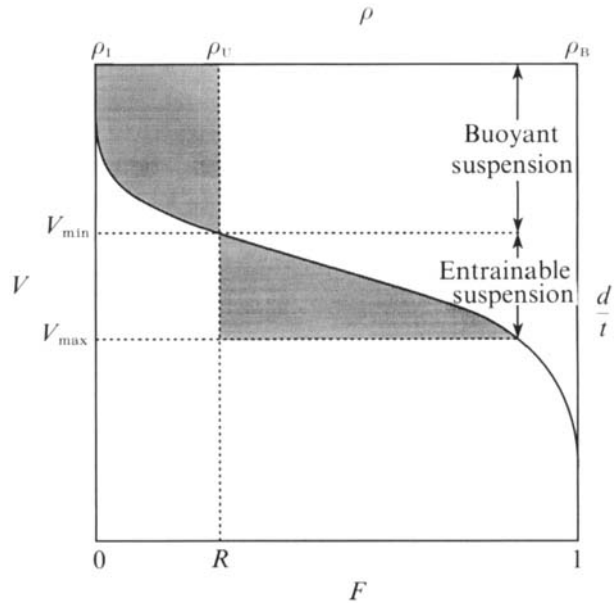

FIGURE 2. A typical (cumulative) distribution of the fraction $F(V)$ of particles settling at speeds less than V. If the volume fraction of particles is small enough so that hindered settling may be ignored, the curve also indicates the bulk density ρ at a depth d after sedimentation for a time t, plotted in the form of d/t versus $r = (\rho-\rho_I)/(\rho_B-\rho_I)$, where ρ_I and ρ_B are respectively the interstitial density and initial bulk density. When overlain by fluid with density ρ_U (density ratio $R = (\rho_U-\rho_I)/(\rho_B-\rho_I)$), part of the suspension is buoyant and convects into the upper region. If none of the underlying, negatively buoyant parts of the suspension are entrained by the convection then a sharp interface descends at the theoretical minimum velocity V_{min}. The theoretical maximum velocity V_{max} is achieved when the average density of the buoyant and entrained material is equal to ρ_U, which corresponds to the value that makes the areas of the two shaded regions equal.

were able to investigate systematically the influence of a number of factors which were not accessible in the earlier results. These factors include the ratio of the upper-region volume to the initial lower-region volume, the ratio of the density difference between suspension and upper layer to that between lower layer and upper layer, and the vigour of the overlying convection.

We first describe a series of experiments in which the effects of mixing and change of density in the overlying fluid are examined. It is shown that if the initial volume of the suspension is comparable to that of the overlying fluid then changes in the density of the overlying fluid cause the interfacial velocity to decrease with time. However, the interfacial velocity at each instant can be predicted from the density of the well-mixed upper layer. Further experiments quantified the variation in the amount of entrainment with the ratio of density differences $R = (\rho_U-\rho_I)/(\rho_B-\rho_I)$ and with the magnitude of the density difference $\rho_B-\rho_I$. The results are interpreted in terms of a buoyancy-derived efficiency of entrainment and the strength of the overlying convection. In a separate experiment, measurements of the size distributions of the particles that are entrained into the upper layer and of the particles that settle to the base of the tank confirm theoretical predictions of a division of particle sizes by this mechanism of sedimentation-driven convection.

Finally, we observe that stable density gradients are ubiquitous in many natural environments, including the world's oceans and lakes (Knauss 1978; Fischer *et al.* 1979; Gill 1982), the atmosphere (Houghton 1977; Gill 1982) and crystallizing

magma chambers (Sparks, Huppert & Turner 1984). It is of great interest, therefore, to consider the effects of stratification in the overlying fluid on the evolution of the sedimenting and convecting system described above (Kerr 1991). Accordingly, we present experimental observations for the case in which the initial stratification of the overlying fluid is linear. It is shown that penetrative convection erodes the overlying gradient in a number of cycles of decreasing intensity and increasing duration. The experimental observations are found to be in good agreement with a theoretical model of the evolution of the sedimenting layers. We suggest that the phenomenon of sedimentation-driven convection may provide an important mechanism for the mixing and ventilation of shallow seas by turbidity currents (Quadfasel, Kudrass & Frische 1990).

2. Experimental equipment and methods

2.1. *Particles*

The use of irregularly shaped particles in the experiments of HKLT led to some uncertainty in the predicted settling behaviour, both because the settling velocity of isolated particles varied significantly with the orientation of the particle and because the hindered-settling coefficients for non-spherical particles are unknown. We wished, therefore, to use spherical particles in the present experiments and, after considerable searching, decided that suitable particles would be provided by glass impact beads (size range AI, produced by Potters Industries Pty. Ltd., Melbourne). In order to obtain a reasonably narrow distribution of particles that were sufficiently small to settle at low Reynolds number in water, we eliminated the largest of the glass particles by first using a 38 μm sieve, and then by repeatedly suspending the sediment in water and decanting only the slowest-settling of the remaining particles. Examination of the final selected particles under a microscope revealed that the vast majority were very nearly spherical though perhaps 1 in 50 were angular shards.

The mean particle density ρ_p was determined to be 2.47 ± 0.02 g cm^{-3} by measuring the bulk density of a suspension which contained a known mass fraction of particles by hydrometer. The distribution of settling velocities was determined by the sedigraph technique (Jones, McCave & Patel 1988) and is shown in figure 3. The median settling velocity in water at 20 °C was 26.4 mm min^{-1}, which corresponds to a median diameter of 23.5 μm and particle Reynolds number of 0.010; the standard deviation in the particle diameter was about 6 μm.

HKLT describe how the distribution of settling velocities may be used to calculate the differential sedimentation of the particles and the consequent evolution of the bulk-density profile. We made a test of the empirical hindered-settling function $\mathscr{F}(\phi) = (1-\phi)^5$ (Davis & Birdsell 1988) used in their calculations by measuring the accumulation of sediment at the base of an initially well-mixed suspension. The laboratory observations are in excellent agreement with the calculated predictions (figure 4). From this result we estimate that the evolution of the bulk-density profile due to differential sedimentation can be predicted to within about 3% from the measured particle velocity distribution and the model of HKLT.

2.2. *Experimental procedure*

The experiments were performed in a rectangular Perspex tank of length 30 cm, width 15 cm and height 65 cm. The tank was designed with movable metal barriers at heights of 15 cm and 30 cm, each of which could be slid horizontally to divide the tank into two regions. The initial two-layer configuration was created by filling the

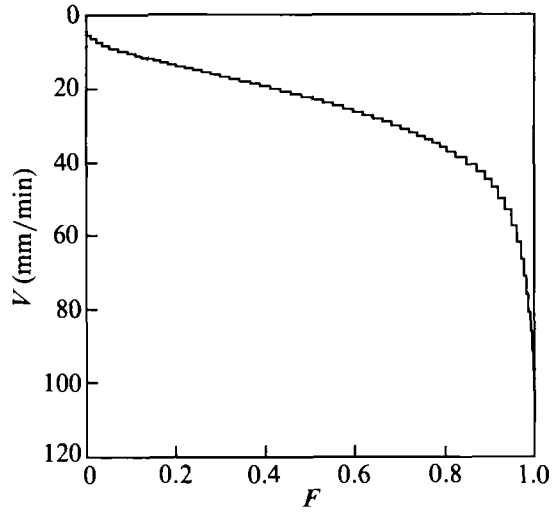

FIGURE 3. The cumulative distribution (by volume) of the settling velocity of the glass beads in water at 20 °C. The distribution is shown discretized since both the original sedigraph measurements and the calculated results are based on discrete particle sizes; we note however that the errors induced by discretization are negligible in comparison with the experimental errors.

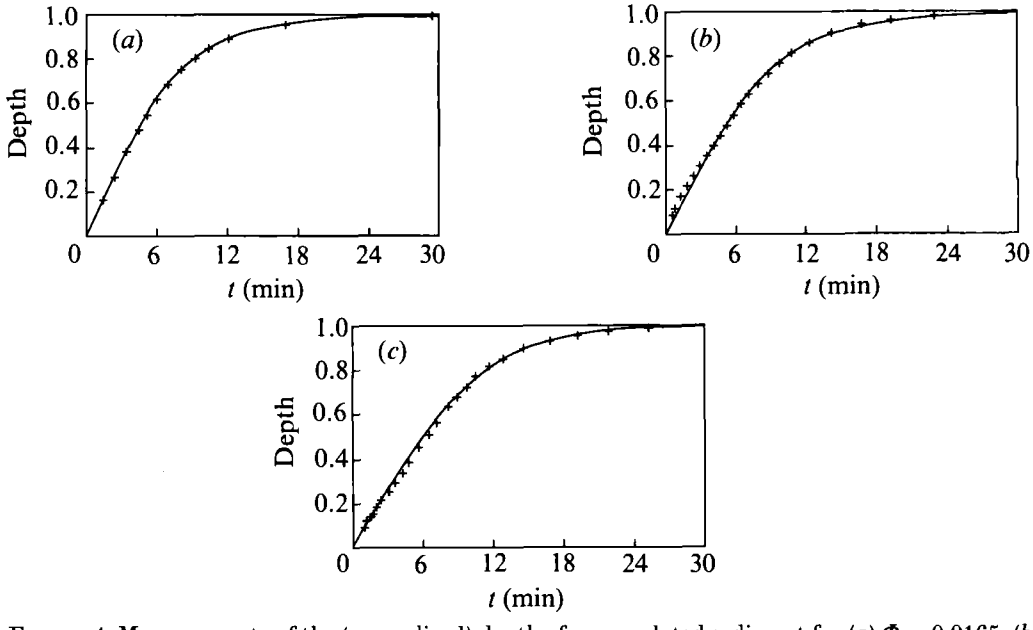

FIGURE 4. Measurements of the (normalized) depth of accumulated sediment for (*a*) $\Phi = 0.0165$, (*b*) $\Phi = 0.0252$, and (*c*) $\Phi = 0.0503$, together with a curve indicating the theoretical predictions based on the velocity distribution given in figure 1 and the theoretical description of HKLT.

tank to the height of one of the barriers with a well-mixed suspension of the particles in water, inserting the barrier, adding an aqueous solution of sugar as the upper layer and then removing the barrier to initiate the experiment. This procedure took about one minute. The subsequent evolution of the experiment was recorded on videotape, enabling accurate and reliable measurements of the interfacial position to be made.

When the interface reached the bottom of the tank, the solution and suspended sediment were rapidly siphoned into a separate container. The sediment was allowed to settle, the (sugar-rich) solution decanted, and fresh water added; a process that was repeated until the concentration of sugar was negligible. The mass of the lifted sediment was then determined from measurements of the mass and bulk density of the resultant freshwater suspension. A similar procedure was applied to obtain the mass of settled sediment. Hence the fraction X of sediment lifted in the experiment could be calculated. We estimate the error in this measurement of X to be less than 0.01.

2.3. *Analysis of results*

In §§3.1–3.2 we discuss the effect of the ratio D_0 of the initial volume of overlying fluid to the initial volume of suspension, which, in our simple rectangular geometry, is given by

$$D_0 = d_U/d_L, \tag{2.1}$$

where d_U and d_L are the initial depths of the upper and lower layers respectively. In the experiments of HKLT $D_0 = 15$, which allowed them to neglect the evolution of the density of the upper layer. In the majority of our experiments $D_0 \leqslant 3$, and mixing with buoyant fluid from the lower layer causes the density of the upper layer, the density ratio

$$R(t) = \frac{\rho_U(t) - \rho_I}{\rho_B - \rho_I}, \tag{2.2}$$

and the interfacial velocity V to vary slowly during the experiment. We note that the use of a spatially uniform value of ρ_U in (2.2) is justified by theoretical estimates of r.m.s. convective velocities (given in the Appendix) and direct observations, both of which show that the overlying convection is sufficiently strong to keep the upper layer well mixed.

In order to compare different experiments, we characterize our results by the values $V_{\frac{1}{2}}$ and $R_{\frac{1}{2}}$ of $V(t)$ and $R(t)$ at the time when the depth of the sedimenting region has decreased to half its initial value. The value of $V_{\frac{1}{2}}$ was determined by least-squares quadratic regression from measurements of the interfacial position with time; the curvature γ of the quadratic fit provides a measure of the variation of V during the experiment. The fraction of sediment lifted during the first half of the experiment may be estimated by the measured value of X at the end of the experiment, from which the value of $R_{\frac{1}{2}}$ can be calculated as

$$R_{\frac{1}{2}} = \frac{2D_0R_0 + X}{2D_0 + 1}. \tag{2.3}$$

Finally, we observe that the relation of $V_{\frac{1}{2}}$ to the theoretical bounds $V_{\min}$ and $V_{\max}$ can usefully be expressed in terms of the extent to which the buoyant plumes of interstitial fluid and suspended sediment are able to entrain some of the underlying negatively buoyant suspension. Relative to the density of the upper layer, the dimensionless buoyancy of a region of bulk density ρ is given by $R - r$, where $r = (\rho - \rho_I)/(\rho_B - \rho_I)$. Analyses of differential sedimentation (Kynch 1952; Smith 1966; Davis & Hassan 1988; etc.) show that r, and ρ, are a function of $v = d/t$, where d is the distance below the original position of the top of the suspension. Thus the minimum interfacial velocity, corresponding to no entrainment of negatively buoyant fluid, is defined by $r(V_{\min}) = R$ and the maximum velocity, corresponding to maximum entrainment of negatively buoyant fluid, is defined such that the average

value of $R-r(v)$ in $0 < v < V_{\max}$ is zero (figure 2). Hence we define an efficiency of entrainment E to be the ratio of the negative buoyancy of the entrained material to the positive buoyancy of the unstable material:

$$E = -\frac{\int_{V_{\min}}^{V_{\frac{1}{2}}} [R_{\frac{1}{2}} - r(v)]\,\mathrm{d}v}{\int_{0}^{V_{\min}} [R_{\frac{1}{2}} - r(v)]\,\mathrm{d}v}. \tag{2.4}$$

Thus $E = 0$ corresponds to $V_{\frac{1}{2}} = V_{\min}$ and $E = 1$ to $V_{\frac{1}{2}} = V_{\max}$.

3. Experimental results

In a series of experiments, summarized in table 1, we systematically examined the effects of varying the initial depth ratio D_0, the initial density ratio $R_0 = R(0)$ and the initial volume fraction Φ of particles in the suspension.

The evolution of all the experiments was in many ways similar to that observed in the experiments performed by HKLT. A sharp interface rapidly developed between a lower region of undisturbed sedimentation and an upper region of large-scale vigorous convection driven by small plumes of sediment-rich fresh water detaching from the interface. However, in contrast to the complex convective circulation generated by the complicated tank geometry used by HKLT, the convection in the upper layer of these experiments was homogeneous and vigorous throughout the upper layer. Typical vertical convective velocities were one to two orders of magnitude greater than the settling velocity of the interface. Since the settling velocities of the lifted particles are less than the interfacial velocity (see §4), we would expect both composition and sediment to be very well mixed in the convecting region, as was observed to be the case.

During the experiments, the bulk density of the upper layer decreased steadily due to the convective mixing of buoyant interstitial fluid and sediment into the upper layer. In turn, this caused the velocity of the interface between the sedimenting and convecting regions to decrease steadily, a result that can be seen in a small curvature in plots of measurements of interfacial position versus time and the positive values of γ from the quadratic regression (see table 1).

3.1. *Experiments* 1 *and* 2

The parameters for these two 'control' experiments were $d_{\mathrm{U}} = 45$ cm, $d_{\mathrm{L}} = 15$ cm, $\Phi = 0.018$ and $R_0 = 0.533$. These values provide the starting point in parameter space for an investigation of the effects of D_0, R_o and Φ in which we vary each of these parameters in turn.

The two experiments gave consistent results to within experimental accuracy, as did repeats of later experiments. The increased consistency in results and the reduction in the size of experimental error bars from the experiments of HKLT are probably due to the simplifications in the tank geometry and particle shape.

We note that, in accord with our general remarks above, V decreased from about 2.54 cm min^{-1} to 2.44 cm min^{-1} during the course of the experiment and the value of $R_{\frac{1}{2}}$ calculated from (2.3) was 0.492, significantly less than R_0.

Typical velocities in the vigorously convecting upper layer were of order 2 cm s^{-1}. If we evaluate the theoretical estimate of the r.m.s. convective velocity V_{rms} given in the Appendix for $h = d_{\mathrm{U}} + \frac{1}{2}d_{\mathrm{L}} = 52.5$ cm, $V_{\frac{1}{2}} = 2.50$ cm min^{-1}, $R_{\frac{1}{2}} = 0.492$, $X = 0.2295$,

Expt.	D_0	Φ	R_0	$R_{\frac{1}{2}}$	$V_{\frac{1}{2}}$ (mm min^{-1})	X	γ (mm min^{-2})
1	3	0.0177	0.530	0.488	25.4	0.22	0.113
2	3	0.0184	0.537	0.497	24.5	0.24	0.051
1 & 2	3	0.0180	0.533	0.492	25.0	0.23	0.082
3 & 4	1	0.0178	0.536	0.434	23.4	0.21	0.251
5 & 6	$\frac{1}{3}$	0.0174	0.522	0.296	17.7	0.13	0.266
7	15	0.0177	0.495	0.486	24.8	0.22	0.002
8 & 9	3	0.0175	0.210	0.193	14.3	0.06	0.060
10 & 11	3	0.0174	0.347	0.317	18.2	0.11	0.148
12 & 13	3	0.0177	0.699	0.653	31.1	0.35	0.841
14 & 15	3	0.0173	0.846	0.796	44.8	0.46	4.59
16	3	0.0019	0.530	0.486	23.3	0.20	0.435
17	3	0.0057	0.530	0.485	24.0	0.20	−0.245
18	3	0.0582	0.515	0.478	20.2	0.24	−0.004

TABLE 1. Experimental parameters and results. In some lines of this table, we show the mean results from two experiments with the same values of the parameters D_0, Φ and R_0. In such cases the variation between the experiments was comparable to that between experiments 1 and 2.

$\rho_B - \rho_I = 0.0265$ g cm^{-3} and $\rho_U = 1.0118$ g cm^{-3} we obtain the value 1.3 cm s^{-1}, which is in reasonable agreement with the direct observations. The ratio $A = V_{rms}/V_{\frac{1}{2}}$ is about 32, confirming that the upper layer should be well mixed.

3.2. *Effect of volume ratio D_0: experiments* 1–7

Four experiments were performed with $d_L = 30$ cm and the same values of R_0 and Φ as in experiments 1 and 2. In experiments 3 and 4, $d_U = 30$ cm, which corresponds to a volume ratio $D_0 = 1$, while in experiments 5 and 6 $d_U = 10$ cm so that D_0 was only $\frac{1}{3}$. The smaller values of D_0 led to a greater decrease in R, and hence in V, during the course of an experiment, which resulted in smaller values of $R_{\frac{1}{2}}$, $V_{\frac{1}{2}}$ and X. These observations suggest the physically reasonable conclusion that the interfacial velocity reflects the instantaneous density of the upper layer, and hence support our definition and use of the parameters $R_{\frac{1}{2}}$ and $V_{\frac{1}{2}}$.

A final experiment with these values of R_0 and Φ was performed in the experimental apparatus of HKLT, where $D_0 = 15$ and hence the variation in R during the experiment was minimal. It was not surprising, therefore, that the interface settled at a nearly constant rate, as is indicated in table 1 by the small value of γ. The value of R_0 was deliberately chosen to be close to the value of $R_{\frac{1}{2}}$ for experiments 1 and 2. We found that the interfacial velocity in the experiment was very close to the values of $V_{\frac{1}{2}}$ for experiments 1 and 2. The values of X are also close. These results suggest that the differences in tank geometry have little effect other than through D_0.

3.3. *Effect of density ratio R: experiments* 1, 2 *and* 8–15

In these experiments we varied the density of the upper layer, while keeping the values of Φ and D_0 fixed. The vigour of the convection in the upper layer was observed to increase systematically with $R_{\frac{1}{2}}$, with convective velocities ranging from about 1 cm s^{-1} for experiments 8 and 9 up to about 3 cm s^{-1} in experiments 14 and 15. This result is reasonably consistent with (A3), which predicts values of 0.9 cm s^{-1} and 1.8 cm s^{-1} respectively.

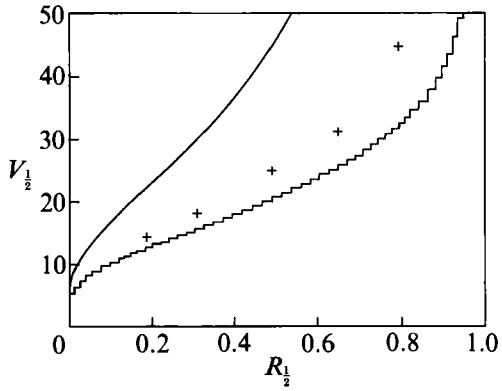

FIGURE 5. The interfacial velocities $V_{\frac{1}{2}}$ (+) observed in experiments with $D_0 = 3$ and $\Phi \approx 0.0176$ as a function of the density ratio $R_{\frac{1}{2}}$. The curves indicate the bounding velocities, $V_{\min}$ and $V_{\max}$, that are predicted by the theoretical description of HKLT. The step-like nature of the lower bounds results from the discrete representation of the distribution of settling velocity shown in figure 1.

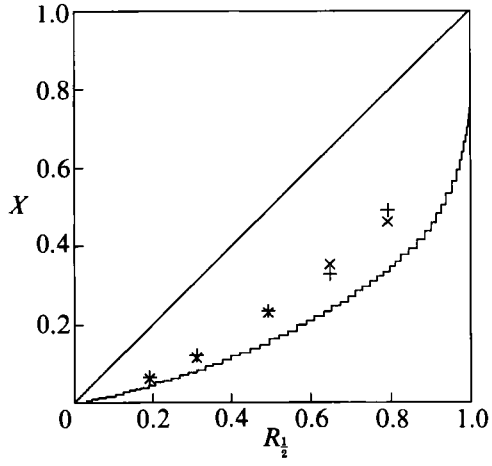

FIGURE 6. Measurements (×) of the fraction X of lifted particles in the experiments shown in figure 4 as a function of the density ratio $R_{\frac{1}{2}}$. Also shown are the values (+) calculated from the observed velocity $V_{\frac{1}{2}}$ and curves giving the bounds, $X_{\min}$ and $X_{\max}$, predicted by the theoretical model of HKLT.

Experiments 10 and 11 were chosen to have values of $R_{\frac{1}{2}}$ similar to those for experiments 5 and 6, and yielded a value of $V_{\frac{1}{2}}$ that was also similar. This result further supports our belief that the interfacial velocity reflects the instantaneous density ratio $R(t)$.

The decrease in the interfacial velocity during the course of an experiment was largest in the experiments with the largest values of R_0, as can be seen from table 1 by the size of γ. This result reflects, firstly, the large decrease in R during these experiments, and secondly, the fact that even a small change in cumulative frequency on the tail of the size distribution in figure 3 results in a large change in sedimentation velocity.

The experimental observations of interfacial velocity $V_{\frac{1}{2}}$, averaged over each pair of experiments, are given as a function of $R_{\frac{1}{2}}$ in figure 5. Also plotted on the figure are curves indicating the maximum ($V_{\max}$) and minimum ($V_{\min}$) bounds on this velocity predicted by the theoretical description of HKLT. The velocities are all seen to lie

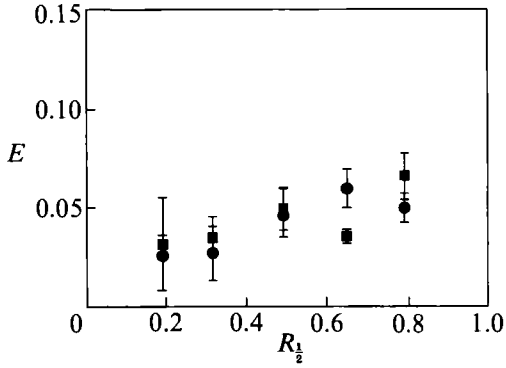

FIGURE 7. The efficiency of entrainment E as a function of the density ratio $R_{\frac{1}{2}}$, for the experiments shown in figure 4. The values are deduced from both the interfacial velocity (■) and the lifted fraction (●).

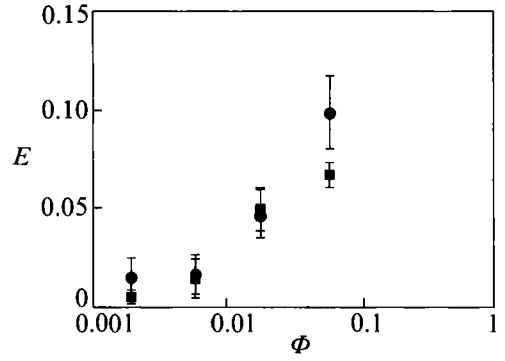

FIGURE 8. The efficiency of entrainment E as a function of the volume fraction of sediment Φ, for the experiments with $D_0 = 3$ and $R_{\frac{1}{2}} \approx 0.485$. The values are deduced from both the interfacial velocity (■) and the lifted fraction (●).

comfortably between the theoretical bounds. In figure 6 the lifted fractions consistent with these interfacial velocities

$$X = V_{\max}^{-1}(V_{\frac{1}{2}}) \tag{3.1}$$

are plotted, together with the measured lifted fractions and the appropriate theoretical bounds. The independent observations of $V_{\frac{1}{2}}$ and X are seen to be in good agreement.

Finally, we observe that the experimental values of E, shown in figure 7, are found to be small and typically about 5%. The figure also suggests that the efficiency is an increasing function of $R_{\frac{1}{2}}$, which may reflect the increasing vigour of the convection in the upper layer.

3.4. *Effect of volume fraction* Φ: *experiments* 1, 2 *and* 16–18

In these experiments we kept the values of $R_{\frac{1}{2}}$ and D_0 fixed and varied the value of Φ. The vigour of the convection in the upper layer was observed to increase systematically with Φ with convective velocities ranging from about 0.5 cm s^{-1} in experiment 16 up to about 3 cm s^{-1} in experiment 18. This result is reasonably consistent with (A3), which predicts values of 0.6 cm s^{-1} and 1.8 cm s^{-1} respectively.

The experimental values of E, plotted in figure 8 as a function of log (Φ), are again found to be small. The figure shows that E is an increasing function of Φ, which again

may reflect the increase in the vigour of the convection in the upper layer with Φ. Further discussion is given in the Appendix.

4. Lifted and settled distributions

We have noted that, as a well-mixed polydisperse suspension starts to sediment, a gradient in particle concentration is created at the top of the lower layer due to differential sedimentation. Large particles fall rapidly away from the top of the layer and so the uppermost parts of the gradient contain only small, slowly settling particles. Since it is the upper part of the gradient that is buoyant due to the low particle concentrations and hence convects into the overlying layer (figure 2), we would expect that the size distribution of the fraction X of particles that are lifted would contain a greater proportion of small particles than the fraction $1-X$ that settle during the fall of the interface.

Accordingly, we performed a number of experiments to examine the size distributions of the particles that were lifted and settled. For a narrow initial size distribution, such as that described in §2.1 and used in the experiments of §3, the separation between the lifted and settled distributions is expected to be small. Therefore, in order to emphasize the separation, we produced a broader size distribution of particles (figure 9*a*) by mixing a sample of the particles described above with a sample of the larger particles that had been earlier separated by sieving. The increase in the median particle diameter necessitated the use of a viscous 47 wt.% sugar solution as the interstitial fluid in order that the particles fell at a sufficiently low Reynolds number in the sedimenting region. Though an even more viscous sugar solution was used in the upper layer, the overlying convection was still vigorous and kept the upper layer well mixed. The experimental parameters were $d_U = 45$ cm, $d_L = 15$ cm, $\rho_U = 1.2245$ g cm^{-3}, $\rho_B = 1.235$ g cm^{-3}, $\rho_I = 1.214$ g cm^{-3} and $T = 20$ °C, corresponding to $\mu_I = 0.115$ g cm^{-1} s^{-1}, $\Phi = 0.0167$ and $R_0 = 0.500$. The measurements yielded values of $V_{\frac{1}{2}} = 5.1$ mm min^{-1}, $X = 0.28$ and $R_{\frac{1}{2}} = 0.469$. This value of $V_{\frac{1}{2}}$ corresponds to the settling velocity of a 38 μm particle. (The correction due to hindered settling at a local volume fraction $\phi = R_0\Phi$ is much less than the uncertainties in distribution described below.)

The sedigraph measurements of the initial, lifted and settled distributions are shown in figure 9*a*. We note that the measurement errors in these distributions were unfortunately significantly greater than those associated with the narrow distribution in figure 3. The size of these errors was estimated by repeated measurements of the same distribution, and by comparison of the initial distribution and a 28:72% mixture of the lifted and settled measurements (figure 9*b*). Despite these uncertainties, it is clear from figure 9(*a*) that there is a marked separation between the lifted and settled distributions and that both differ significantly from the initial distribution. It should be pointed out that, even without convection in an overlying layer, differential sedimentation would produce a natural grading of the sedimented pile in which the proportion of large particles increases smoothly towards the bottom of the pile due to their greater settling velocities. In the present case, the lifted distribution is mixed by the convection until the interface reaches the bottom, convection ceases and the lifted particles are free to settle. An important implication of this mixing is that a discontinuity in the size distribution within the sedimented pile is generated at the height corresponding to the end of the convective phase. Such discontinuities may be reflected in the layering of turbidites (Stow & Piper 1984) and ignimbrites (Wilson 1986).

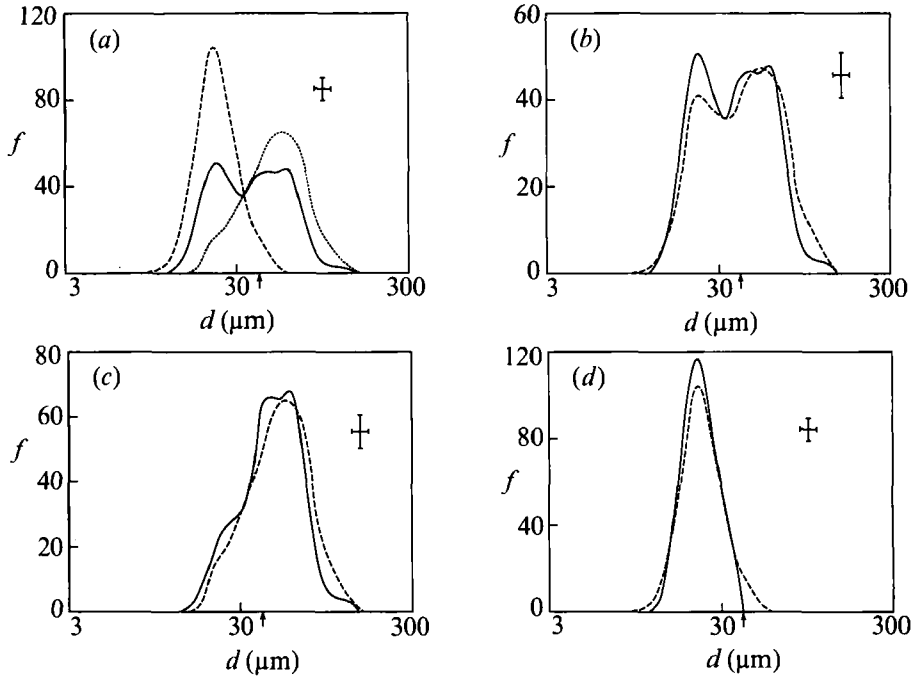

FIGURE 9. Probability density functions f for the distribution of particle diameters d. The cumulative distribution is given by $\int f(p)\,dp$, where $p = \log_{10} d$ (p corresponds to the 'phi-scale' used in sedimentology). Estimated error bars are as marked. (*a*) The initial (——), lifted (– – – –) and settled (- - - - - -) distributions from an experiment with $R_0 = 0.50$, $\Phi = 0.0167$ and in which the observed interfacial velocity $V_{\frac{1}{2}}$ is equal to the settling velocity of a particle with a diameter of 38 μm (indicated on the axis by ↑). (*b*) Comparison of the initial distribution (——) with a $X:1-X$ mixture (– – – –) of the measured lifted and settled distributions. (*c*) Predicted (——) and observed (– – – –) settled distributions. (*d*) Predicted (——) and observed (– – – –) lifted distributions.

The detailed stratification in the final layered deposit can be calculated from the description of differential settling given by HKLT. If hindered settling effects and the variation of V with time are both negligible then it is straightforward to calculate the depth-averaged distributions of the lifted and settled particles as follows. The duration of the experiment is given by $d_L/V_{\frac{1}{2}}$. During this time all particles with settling velocities $u > V_{\frac{1}{2}}$ and a proportion $u/V_{\frac{1}{2}}$ of particles with settling velocities $u < V_{\frac{1}{2}}$ will have had time to settle. Similarly, the lifted distribution is composed of a proportion $1-u/V_{\frac{1}{2}}$ of the particles with settling velocities $u < V_{\frac{1}{2}}$. Thus, the lifted and settled distributions may be derived from the initial distribution. We observe that the settled distribution contains particles of all sizes (though fewer of the smaller sizes), whereas the lifted distribution contains only particles with $u < V_{\frac{1}{2}}$. The lifted and settled distributions predicted from the initial distribution of particle sizes in our experiment are shown in figures 9(*c*) and 9(*d*). The predictions agree reasonably well with the observations though, as we have noted, there is considerable uncertainty in the experimental measurements.

5. Sedimentation below a density gradient

Motivated by the widespread occurrence of stable density gradients in nature, we investigated the evolution of a dense suspension emplaced below a stably stratified upper layer for the case in which the interstitial fluid density is less than that of the

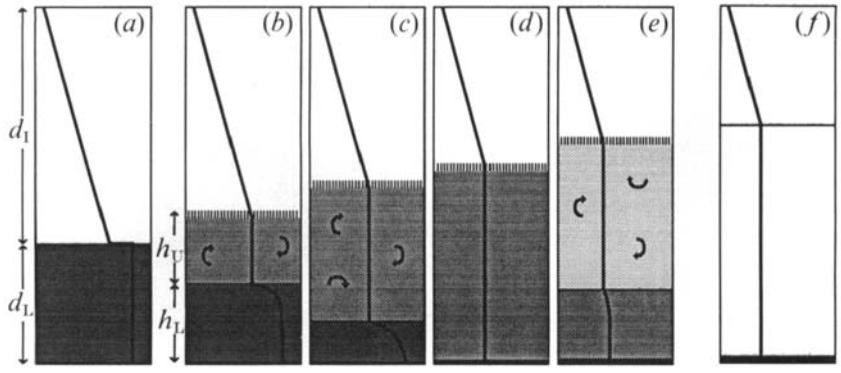

FIGURE 10. Schematic representation of the cycles of coupled sedimentation and convection, and the corresponding changes in the bulk-density profile, that occur when a suspension is emplaced underneath a density gradient (see text for a detailed description).

overlying gradient. In a series of experiments an initial two-layer configuration was established as follows. First, a stratified upper layer composed of an aqueous sugar solution was produced using the double-bucket technique (Oster & Yamamoto 1963; Oster 1965). Then a lower-layer suspension of the glass particles described in §2.1 in water was rapidly added below the sugar gradient using a pipe leading from a well-mixed reservoir to the bottom of the experimental tank. The motion in the lower layer generated during input was observed to be rapidly dissipated and measurements of refractive index showed that there was very little mixing between the layers during input. However, sedimentation in the lower layer and the release of the light interstitial fluid soon initiated convective motion in the overlying fluid.

The evolution of the experiments is shown schematically in figure 10, commencing in figure 10(*a*) with the initial condition of a stratified layer underlain by a suspension. As in the unstratified case, there was undisturbed sedimentation in the lower layer which was separated from overlying convection by a sharp, descending interface. However, owing to the stratification, the vigorously convecting region did not extend through the depth of the upper layer, but was confined to a smaller depth immediately above the suspension (figure 10*b*). As buoyant fluid was released from the underlying suspension, the bulk density of the well-mixed convecting region decreased steadily, leading to the erosion of the overlying density gradient (figure 10*c*). In contrast to the sharp interface at the base of the convecting region, the interface between the convecting region and the uneroded gradient was diffuse (typically 2 cm thick). The interface consisted of narrow vertical protrusions of buoyant, sediment-rich fluid intruding into the gradient (figure 11), which were occasionally disrupted by large diapirs rising from the convecting region. The protrusion region contrasts markedly with observations of 'domes', 'cusps', 'folds' and 'waves' in the entrainment zone when a stable thermal gradient is heated from below (Deardorff, Willis & Lilly 1969; Deardorff, Willis & Stockton 1980). The protrusions look similar to double-diffusive 'salt fingers' (Turner 1973; Green 1987), but the physics of their formation is fundamentally different as it does not involve diffusion. We suggest that the protrusions develop from a local gravitational instability at the top of the convecting region. The instability arises because the vertical turbulent convective velocities decrease towards the top of the convecting region, thus allowing sedimentation to occur and the local bulk density to decrease.

The convecting region continued to grow at the expense of both the underlying

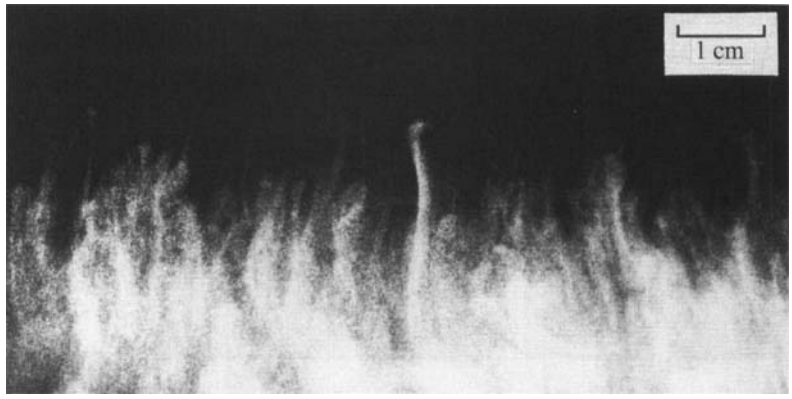

FIGURE 11. Photograph of the buoyant, particle-laden protrusions that penetrate the stable stratification at the top of the convecting layer. The photograph shows the light scattered by individual particles when the tank is illuminated at right angles to the line of sight.

sedimenting region and overlying gradient until the descending sharp interface reached the base of the tank and the generation of buoyancy at the base of the convecting region ceased. The convective motions rapidly dissipated, leaving a situation (figure 10*d*) similar to figure 10(*a*): namely, a well-mixed region of light fluid and sediment underlying a gradient (although it should be noted that the sediment concentration was much reduced and the density of the interstitial fluid was now greater than ρ_I due to mixing of the light interstitial fluid with the lower part of the gradient). Hence it was not surprising that a new sharp interface developed as part of another cycle of coupled sedimentation and convection (figure 10*e*). This second cycle was slower, the convection weaker, and the erosion of the gradient less. At the end of the second cycle, the concentration of suspended sediment was very small (less than 1% of its initial value) so that, although further cycles seemed plausible, they could not be discerned. After a long time, all the sediment had settled, and the final state shown in figure 10(*f*) was reached.

The experimental observations can be analysed by generalizing the theoretical description of the simpler unstratified case given in earlier sections. Observation and the magnitude of convective velocities show that the convecting region is well mixed with a uniform bulk density ρ_U. Owing to the addition of buoyant fluid from below and the erosion of the overlying gradient, ρ_U decreases with time, so that $R(t)$ (defined by (2.2)) also decreases with time. Based on our successful use of $R_{\frac{1}{2}}$ and $V_{\frac{1}{2}}$ to parameterize the experiments of §3, we assume that both the velocity $V(t)$ of the interface at the base of the convecting region and the current fraction $X(t)$ of particles being lifted are known functions of the instantaneous value of $R(t)$. With this assumption, it is straightforward to calculate the evolution of the system.

We define $h_L(t)$ and $h_U(t)$ to be the depths of the sedimenting and convecting regions during the first cycle of sedimentation and convection. Thus,

$$\frac{\mathrm{d}h_L}{\mathrm{d}t} = -V(R), \tag{5.1}$$

$h_L(0) = d_L$ and $h_U(0) = 0$. The diffuse nature of the interface between the convecting region and the overlying gradient suggests that h_U increases by passive incorporation of the gradient and hence that the density at the base of the uneroded gradient is equal to ρ_U. Therefore, if the density gradient is given by $\rho(z) = \rho_{U_0} - (\rho_{U_0} - \rho_I)(z/d_I)$,

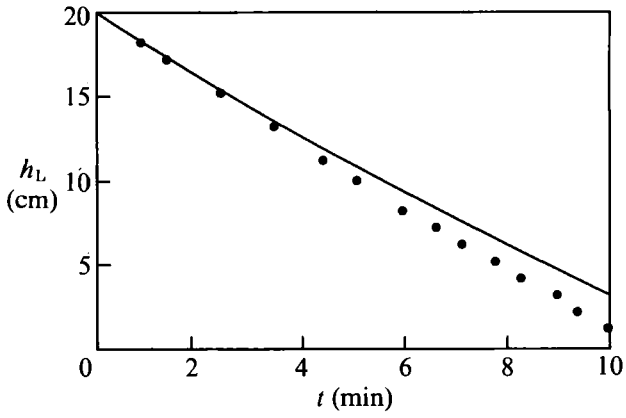

FIGURE 12. Theoretical prediction and experimental values (●) of the position of the sharp interface between the convecting and sedimenting layers during the first cycle (figure 10*b*, *c*) of simultaneous sedimentation and convection. The gradual deviation of the prediction from the observations indicates a steady increase in E from almost zero to about 0.025 at the end of the experiment.

where z is the height above the initial interface between the two layers and d_I defines the strength of the gradient, then the continuity of density at $z = h_U + h_L - d_L$ implies that

$$R(t) = R_0\left(1 - \frac{h_U + h_L - d_L}{d_I}\right). \tag{5.2}$$

However, $R(t)$ can also be calculated from the density of the mixture of the buoyant fluid released from the sedimenting region and the incorporated part of the gradient. In differential form this calculation relates h_U and h_L by

$$\frac{\mathrm{d}h_U}{\mathrm{d}h_L} = \frac{d_I(1 - X(R)/R_0) + h_L - d_L}{h_U}. \tag{5.3}$$

Given the functions $V(R)$ and $X(R)$, equations (5.1)–(5.3) can be integrated numerically to determine $h_U(t)$ and $h_L(t)$ during this first cycle. The subsequent cycles may be analysed in an entirely analogous manner using the initial conditions from the previous cycle. In the final state (figure 10*f*), after all cycles of convection have taken place and all particles have sedimented, there is a layer of fluid of uniform density underlying the remaining uneroded gradient. The density of the uniform layer can be calculated from the mixing of the initial interstitial fluid and the eroded part of the gradient. Hence the depth of this layer is given by

$$h_U(\infty) = d_L(1 + 2d_I/d_L)^{\frac{1}{2}}. \tag{5.4}$$

This description of the evolution of the layers was tested against observations from an experiment in which $\rho_B = 1.034$ g cm^{-3}, $\rho_I = 0.999$ g cm^{-3}, $\rho_{U_0} = 1.020$ g cm^{-3}, $d_L = 20$ cm and $d_I = 40$ cm. For simplicity, and based on the small values of E in §3, we assumed that V and X are given by the lower bounds $V_{\min}$ and $X_{\min}$. The calculated position of the sharp interface versus time is shown in figure 12 together with the experimental observations. The agreement at early times is excellent, while at later times the interfacial velocity is somewhat greater than $V_{\min}(R)$. This systematic departure is probably due to the steady increase in h_U, which increases the vigour of convection and hence the value of E (see §§3.3 and 3.4).

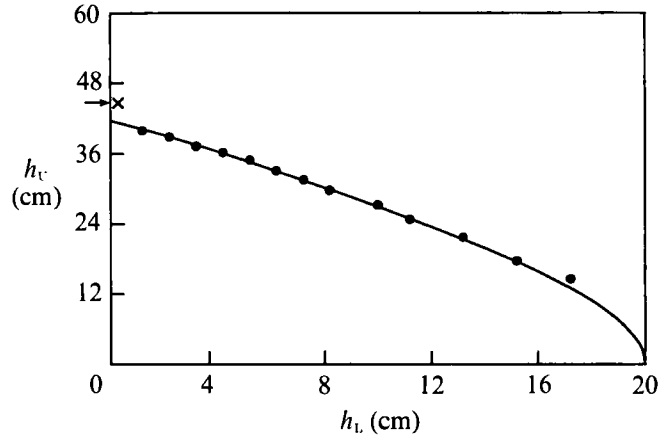

FIGURE 13. Theoretical prediction and experimental values (●) for the depth of the convecting region h_U as a function of the depth of the sedimenting region h_L during the first cycle. Also shown is the final extent of gradient erosion after several cycles of convection have led to the settling of all the sediment (×) together with the theoretical prediction (→) of (5.4).

In figure 13 we present the theoretical prediction of h_L as a function of h_U together with the experimental observations. It may be seen that (5.1)–(5.3) accurately predict the position of the top of the protrusion interface. Also shown in this figure is the final depth of the well-mixed region, which is in good agreement with the prediction of (5.4).

A number of further predictions may be derived from the model described above. An analogous calculation to that presented in §4 yields the concentration and size distribution of the particles lifted into the convecting region. These values can be used to predict the evolution of the second (figure 10*e*) and subsequent convective cycles. The convection and gradient erosion in these later cycles is much weaker owing to the small particle sizes, large suspension depths and low sediment concentrations that remain at the end of the first cycle. It will be noted from §4 that the size distribution of the particles that are lifted in each cycle differs from the size distribution of the particles that settle in that cycle. It follows that each cycle generates a discontinuity in the variation of size distribution with height in the final settled sediment.

6. Conclusions

In this paper we have extended the recent investigations by HKLT of the simple two-layer system where a suspension is emplaced beneath a fluid whose density is greater than that of the interstitial fluid but less than that of the bulk suspension. This initially stable situation is unstable because sedimentation of the dense particles within the suspension leaves behind buoyant interstitial fluid that drives vigorous convection in the overlying fluid. In the current paper we quantify this fundamental phenomenon in a series of careful experiments using suspensions of spherical glass beads in a simple rectangular geometry.

In our experiments, the convective velocities in the overlying fluid, which we estimate in an Appendix, were much larger than the settling velocities of the particles, and as a result the convecting region was well mixed in both composition and particle concentration. Our experiments demonstrate that sedimentation and

convection in this system are intimately coupled: the instantaneous value of the bulk density of the well-mixed region determines which parts of the underlying sedimenting suspension are buoyant and hence determines the rate of descent of the sharp interface that separates the two regions, while the interfacial velocity in turn determines the rate at which buoyant fluid (and some of the finer sediment) is mixed into the convecting region and hence the rate at which its bulk density decreases.

Our experiments have determined the energetic efficiency with which the buoyant parts of the suspension are able to entrain the underlying, negatively buoyant parts as they convect away. We find that this efficiency is small, typically about 5%, and that it seems to increase as the vigour of the overlying convection increases.

In many natural applications, for example to turbidity currents in oceans (Quadfasel *et al.* 1990), freshwater lakes (Gilbert 1975; Gustavson 1975) and reservoirs (Gould 1960), the suspension will be typically overlain by a fluid that is stratified rather than homogeneous. In this case, our experiments show that the base of the density gradient is eroded to form a well-mixed convecting layer that grows at the expense of both the underlying sedimenting region and the overlying remaining gradient. When the initial sedimenting region has been lost, convection in the well-mixed layer ceases and sedimentation begins again, leading to a new cycle of coupled sedimentation and convection. Our experimental observations of this interesting evolution are accurately predicted by a simple extension of the model of HKLT. Given the initial fluid and suspension properties, this model can be readily applied to situations such as the turbidity currents inferred by Quadfasel *et al.* (1990), for which it can be used to predict the rate and extent of vertical mixing as well as the variation of the particle size distribution with depth, including discontinuities, in the final turbidite.

We are grateful to Tony Beasley, Derek Corrigan and Ross Wylde-Browne of the Research School of Earth Sciences for their superb technical assistance with the laboratory experiments, and to David Fredericks and Gary Caitcheon of the CSIRO Division of Water Resources and Gillian Foreman of the Earth Sciences Department in Cambridge for the sedigraph measurements of our particles. We thank Herbert Huppert, Don Koch and Stewart Turner for many helpful comments on the manuscript.

Appendix. Scaling arguments for the upper-layer convection

The convective motion in the upper layer is driven by the release of light fluid with mean density deficit $\Delta\rho = (\rho_B - \rho_I)(R_{\frac{1}{2}} - X)$ at the base of the upper layer due to the downward motion of the sedimentation front. The timescale Δt and thickness Δh associated with detachment of the growing layer of light fluid into the overlying convection can be estimated by equating the growth rate of the Rayleigh–Taylor instability of the buoyant layer (e.g. Selig 1965; Lister & Kerr 1989) to the growth rate of the layer itself (cf. the treatment of thermal boundary-layer detachment by Lick 1965 and Howard 1966). We obtain

$$\Delta t \sim (\nu/Vg')^{\frac{1}{2}}, \quad \Delta h \sim (V\nu/g')^{\frac{1}{2}}, \tag{A 1}$$

where ν is the kinematic viscosity of the fluid and $g' = g\Delta\rho/\rho_U$. In our experiments these scales had typical values of a few millimetres and a few seconds, which are much less than the scales h and h/V characteristic of the evolution of the system. Hence the convection in the upper layer is driven by frequent detachment of a thin

layer of buoyant fluid at its base and the flow is thus expected (and observed) to be similar to high-Rayleigh-number thermal convection with comparable buoyancy flux.

In order to predict the convective velocities driven by the release of light fluid at the base of the upper layer, we consider previous results for thermal convection driven from only one boundary. Martin (1988) applied the scaling arguments of Kraichnan (1962) to show that the mid-depth r.m.s. vertical velocity is given by

$$V_{\rm rms} \sim (g\alpha q h/(2\rho c_P))^{\frac{1}{3}}, \tag{A 2}$$

where α is the coefficient of thermal expansion, q is the vertical heat flux, h is the height of the layer, and ρ and c_P are respectively the density and heat capacity of the fluid. Martin then extended earlier experimental data sets (Malkus 1954; Garon & Goldstein 1973) and verified (A2) for flux Rayleigh numbers $Ra_{\rm f} = g\alpha q h^4/(\kappa^2 \mu c_P)$ between 10^7 and 10^{11}, where κ is the thermal diffusivity. The constant of proportionality was estimated to be 0.7 with an uncertainty of about 20% and no apparent variation with Prandtl number in the range $5 \leqslant Pr = \nu/\kappa \leqslant 100$. It will be noted that the r.m.s. velocity does not depend on κ, consistent with the idea that the motion depends primarily on the buoyancy flux and not on the mechanism of release.

In order to apply (A2) to our experiments, the thermal buoyancy flux $g\alpha q/c_P$ should be replaced by the effective buoyancy flux $gV\Delta\rho$ released at the interface to obtain the estimate

$$V_{\rm rms} \approx 0.7\,(\tfrac{1}{2} g' V h)^{\frac{1}{3}}. \tag{A 3}$$

Since the settling velocities of the lifted particles will be at most comparable to the interfacial velocity, a useful measure of the extent to which the lifted particles are well-mixed in the upper layer is given by the ratio

$$A \equiv V_{\rm rms}/V \approx 0.7\,(g' h/(2V^2))^{\frac{1}{3}}. \tag{A 4}$$

In all our experiments $A \gg 1$ indicating that the lifted particles should be well mixed. This was observed to be the case.

It is rather more difficult to obtain a scaling estimate of E since this does depend on the detailed mechanism of detachment, and is probably influenced by the overlying turbulent flow (Castaing *et al.* 1989).† From (A1) and (A4) it is clear that E will thus depend on g', V, etc., from which we can construct the dimensionless groups $g'h^3/\nu^2$, hV/ν, $Sc = \nu/\kappa_{\rm s}$ and Φ, where $\kappa_{\rm s}$ is the diffusivity of sugar. Least-squares regression from the values obtained in the experiments with $D_0 = 3$ shows that the dependence on Φ is felt primarily through g' and that the data are well represented by

$$E \propto (g'h^3/\nu^2)^{0.677 \pm 0.075}\,(hV/\nu)^{0.064 \pm 0.203}, \tag{A 5}$$

where the constant of proportionality is an unknown function of the Schmidt number Sc. We have been unable to find a mechanistic explanation for the dependence on h and the apparent weakness of the dependence on V.

REFERENCES

Castaing, B., Gunaratne, G., Heslot, F., Kadanoff, L., Libchaber, A., Thomae, S., Wu, X.-Z., Zaleski, S. & Zanetti, G. 1989 Scaling of hard thermal turbulence in Rayleigh–Bénard convection. *J. Fluid Mech.* **204**, 1–30.

Davis, R. H. & Birdsell, K. H. 1988 Hindered settling of semi-dilute monodisperse and polydisperse suspensions. *AIChE J.* **34**, 123–129.

† The influence of the overlying flow is further made plausible by the observation of wave-like motions on the interface, driven by the impingement of large eddies from above (see HKLT). These waves may interact weakly with the boundary-layer detachment, which occurred on smaller scales.

DAVIS, R. H. & HASSEN M. A. 1988 Spreading at the interface at the top of a slightly polydisperse sedimenting suspension. *J. Fluid Mech.* **196**, 107–134.

DEARDORFF, J. W., WILLIS, G. E. & LILLY, D. K. 1969 Laboratory investigation of non-steady penetrative convection. *J. Fluid Mech.* **35**, 7–31.

DEARDORFF, J. W., WILLIS, G. E. & STOCKTON, B. H. 1980 Laboratory studies of the entrainment zone of a convectively mixed layer. *J. Fluid Mech.* **100**, 41–64.

FISCHER, H. B., LIST, E. J., KOH, R. C. Y., IMBERGER, J. & BROOKS, N. H. 1979 *Mixing in Inland and Coastal Waters.* Academic.

GARON, A. M. & GOLDSTEIN, R. J. 1973 Velocity and heat transfer measurements in thermal convection. *Phys. Fluids* **16**, 1818–1825.

GILBERT, R. 1975 Sedimentation in Lillooet Lake, British Columbia. *Can. J. Earth Sci.* **12**, 1697–1711.

GILL, A. E. 1982 *Atmosphere–Ocean Dynamics.* Academic.

GOULD, H. R. 1960 Turbidity currents. In *Comprehensive Survey of Sedimentation in Lake Mead, 1948–1949. Prof. Pap. US Geol. Surv.*, vol. 295, pp. 201–207.

GREEN, T. 1987 The importance of double diffusion to the settling of suspended material. *Sedimentology* **34**, 319–331.

GUSTAVSON, T. C. 1975 Bathymetry and sediment distribution in proglacial Malaspina Lake, Alaska. *J. Sed. Petrol.* **45**, 450–461.

HOUGHTON, J. T. 1977 *The Physics of Atmospheres.* Cambridge University Press.

HOWARD, L. N. 1966 Convection at high Rayleigh number. In *Proc. 11th Intl Congr. Appl. Mech., Munich*, pp. 1109–1115. Springer.

HUPPERT, H. E., KERR, R. C., LISTER, J. R. & TURNER, J. S. 1991 Convection and particle entrainment driven by differential sedimentation. *J. Fluid Mech.* **226**, 349–369 (referred to herein as HKLT).

JONES, K. P. N., MCCAVE, I. N. & PATEL, P. D. 1988 A computer-interfaced sedigraph for modal size analysis of fine-grained sediment. *Sedimentology* **35**, 163–172.

KERR, R. C. 1991 Erosion of a stable density gradient by sedimentation-driven convection. *Nature* **353**, 423–425.

KNAUSS, J. A. 1978 *Introduction to Physical Oceanography.* Prentice-Hall.

KRAICHNAN, R. H. 1962 Turbulent thermal convection at arbitrary Prandtl number. *Phys. Fluids* **5**, 1374–1389.

KYNCH, G. J. 1952 A theory for sedimentation. *Trans. Faraday Soc.* **48**, 166–176.

LICK, W. 1965 The instability of a fluid layer with time dependent heating. *J. Fluid Mech.* **21**, 565–576.

LISTER, J. R. & KERR, R. C. 1989 The effect of geometry on the gravitational instability of a buoyant region of viscous fluid. *J. Fluid Mech.* **202**, 577–594.

MALKUS, W. V. R. 1954 Discrete transitions in turbulent convection. *Proc. R. Soc. Lond.* A **225**, 185–195.

MARTIN, D. 1988 Fractional crystallization in convecting magma chambers. Ph.D. thesis, Australian National University.

OSTER, G. 1965 Density gradients. *Sci. Am.* **213**, 70–76.

OSTER, G. & YAMAMOTO, M. 1963 Density gradient techniques. *Chem. Rev.* **63**, 257–268.

QUADFASEL, D., KUDRASS, H. & FRISCHE, A. 1990 Deep-water renewal by turbidity currents in the Sulu Sea. *Nature* **348**, 320–322.

SELIG, F. 1965 A theoretical prediction of salt dome patterns. *Geophysics* **30**, 633–643.

SMITH, T. N. 1966 The sedimentation of particles having a dispersion of sizes. *Trans. Instn Chem. Engrs* **44**, 153–157.

SPARKS, R. S. J., HUPPERT, H. E. & TURNER, J. S. 1984 The fluid dynamics of evolving magma chambers. *Phil. Trans. R. Soc. Lond.* A **310**, 511–534.

STOW, D. A. V. & PIPER, D. J. W. 1984 *Fine-grained Sediments: Deep Water Processes and Facies.* Blackwell.

TURNER, J. S. 1973 *Buoyancy Effects in Fluids.* Cambridge University Press.

WILSON, C. J. N. 1986 Pyroclastic flows and ignimbrites. *Sci. Prog., Oxf.* **70**, 171–207.